Dichloroacetate reverses sepsis-induced hepatic metabolic dysfunction

Rabina Mainali[1*], Manal Zabalawi[2*], David Long[2], Nancy Buechler[1], Ellen Quillen[2], Chia-Chi Key[2], Xuewei Zhu[2], John S. Parks[2], Cristina Furdui[2], Peter W. Stacpoole[3], Jennifer Martinez[4], Charles E. McCall[2#], Matthew A, Quinn[1,2,5#]

[1]Department of Pathology, Section on Comparative Medicine Wake Forest School of Medicine, Winston-Salem, North Carolina

[2]Department of Internal Medicine, Section on Molecular Medicine Wake Forest School of Medicine, Winston-Salem, North Carolina

[3]Division of Endocrinology, Diabetes and Metabolism, Department of Medicine and Department of Biochemistry and Molecular Biology, University of Florida College of Medicine, Gainesville, Florida

[4]Immunity, Inflammation, and Disease Laboratory, National Institute of Environmental Health Sciences (NIEHS), National Institutes of Health (NIH), Research Triangle Park, NC

[5]Lead Contact

* these authors contributed equally
# denotes co-corresponding author

Corresponding Authors:

Matthew A. Quinn, Ph.D.
Wake Forest School of Medicine
Medical Center Blvd
Winston-Salem, NC 27157
Office: 336-713-1995
mquinn@wakehealth.edu

Charles E. McCall, M.D.
Wake Forest School of Medicine
Medical Center Blvd
Winston-Salem, NC 27157
Office: 336 413 8034
chmccall@wakehealth.edu

Keywords: sepsis, mitochondria function, liver, inflammation, metabolism, steatosis

Abstract

Dramatic metabolic reprogramming between an anabolic resistance and catabolic tolerance state occurs within the immune system in response to systemic infection with the sepsis syndrome. While metabolic tissues such as the liver are subject to end-organ damage during sepsis and are the primary cause of sepsis death, how their metabolic and energy reprogramming during sepsis state ensures survival is unclear. Employing comprehensive metabolomic screening, targeted lipidomic screening, and transcriptional profiling in a mouse model of septic shock, we show that hepatocyte lipid metabolism, mitochondrial TCA energetics, and redox balance are significantly reprogramed after cecal ligation and puncture (CLP). We identify increases in TCA cycle metabolites citrate, cis-aconitate, and itaconate with reduced fumarate and triglyceride accumulation in septic hepatocytes. Transcription analysis of liver tissue supports and extends the hepatocyte findings. Strikingly, the administration of the pyruvate dehydrogenase kinase (PDK) inhibitor dichloroacetate (DCA) reverses dysregulated hepatocyte metabolism and mitochondrial dysfunction. Our data indicate sepsis promotes hepatic metabolic dysfunction. Furthermore, our data indicate that targeting the mitochondrial PDC/PDK energy homeostat rebalances transcriptional and metabolic manifestations of sepsis within the liver.

Sepsis is a potentially life-threatening condition that occurs due to the body's overwhelming response to an infection. This reaction leads to aberrant immune responses and if not diagnosed and treated early after its onset, may limit survival by inducing coagulopathy, altered microvasculature, and dysregulation of the host's metabolism and organ function [1-7]. Sepsis accounts for one in three hospital deaths in the U.S. and millions of deaths each year globally, highlighting its hazard to public health [8,9]. The high mortality rate associated with sepsis reflects the lack of a clinically viable molecular-based therapeutic target. Therefore, understanding the pathogenesis of sepsis at both the molecular and organismal level is of utmost importance to address major gaps in knowledge regarding sepsis.

The response to sepsis has classically been characterized as a biphasic phenomenon, where the acute phase is characterized by high energy consumption and hyperinflammation associated with oxidative stress, followed by cellular reprogramming to a low energy, anti-inflammatory state of immunometabolic paralysis, with accompanying organ failure [8,10-12]. Additionally, during the early phase of sepsis increased catabolism of fats, proteins, and carbohydrates, associated with high rates of oxygen consumption and ATP synthesis is observed [13-16]. Following the acute phase is a hypometabolic state where ATP production and mitochondrial respiration decreases [13]. It is postulated that this is a protective mechanism to overall lower the metabolic demands of the cell and help with its recovery [1,17,18].

Of particular interest to us, during the hyper-inflammatory anabolic phase of sepsis, an increase in the expression and activity of pyruvate dehydrogenase kinase 1 (PDK1) consistently occurs [19,20]. This enzyme is one of four PDK isoforms that reversibly phosphorylates serine residues on pyruvate dehydrogenase complex (PDC) E1a subunit, inhibiting the conversion of pyruvate to acetyl coenzyme A (acetyl CoA) [21]. Inhibition of this important enzymatic activity that connects glycolysis to tricarboxylic acid (TCA) cycle, oxidative phosphorylation (OXPHOS), and the lipogenic pathway is thought to be an important mechanism driving the dysfunction of mitochondrial respiration and cell bioenergetics observed during sepsis [19,22]. Therefore, PDK serves as a potential therapeutic target as it can allow for the downstream oxidation of glucose to continue, restoring

OXPHOS and mitochondrial functioning that we know to be altered in both immune and non-immune cells during sepsis [16,19,23,24].

The liver is an important metabolic and immune organ due to its role in nutrient metabolism and production of acute phase proteins. However, our understanding of transcriptional alterations and subsequent metabolic manifestations elicited by sepsis still remain limited [16,25-28]. Furthermore, the effects of DCA at restoring hepatic metabolic function in the context of sepsis is completely unknown. Hence, we set out to characterize the hepatic manifestations of sepsis, with the overall goal of identifying global metabolic pathways subject to dysregulation and whether these pathways are restored by DCA treatment.

126 **Results**
127
128 **Sepsis Impairs Hepatic Mitochondrial Metabolism**

129 To test the long-term hepatic transcriptional changes elicited by sepsis, we
130 performed RNA-seq in whole livers thirty-hours post cecal ligation puncture (CLP). At this
131 time point, septic mice exhibit tolerance, in which immunometaboic paralysis and end
132 organ dysfunctions decrease survival. Ingenuity pathway analysis (IPA) of the top
133 physiological pathways subject to alteration in response to sepsis revealed a significant
134 increase in the acute phase response pathway, highlighting a persistent inflammatory
135 state in the liver into the chronic phase of sepsis (Fig. 1a). Of particular interest were the
136 findings that oxidative phosphorylation and mitochondrial dysfunction were the top two
137 enriched pathways in the liver of septic mice (Fig. 1a). To gain further insight into the
138 effects of sepsis on the transcriptional regulation of mitochondrial function, we performed
139 gene set enrichment analysis (GSEA) of the oxidative phosphorylation pathway
140 (GO:0006119). Septic mice at 30 h decreased the transcriptional output of OXPHOS
141 components, as evidenced by a negative GSEA enrichment score (Fig. 1b). Given the
142 connection between oxidative phosphorylation and the tricarboxylic acid (TCA) cycle, we
143 next asked if polymicrobial infection would elicit similar alterations in this pathway. In
144 accordance with the changes observed in the oxidative phosphorylation pathway, we
145 found a negative enrichment score for TCA cycle enzymes (GO:0006099) in the liver of
146 CLP mice (Fig. 1c). Thus, our transcriptome data indicate that sepsis impairs
147 mitochondrial metabolism in the liver.

148 Next, we wanted to assess if the transcriptional changes elicited by sepsis would
149 manifest in altered hepatic TCA cycle metabolism. Therefore, we performed global

150 unbiased metabolomic screening in isolated hepatocytes from control and septic mice by
151 Ultrahigh Performance Liquid Chromotography-Tandem Mass Spectroscopy (UPLC-
152 MS/MS). In line with altered transcriptional regulation of the TCA cycle, we found that
153 sepsis altered the relative abundance of multiple metabolites involved in the TCA cycle
154 (Fig. 1d). In particular, significant elevation of citrate and cis-aconitate was observed in
155 septic hepatocytes at 30h (Fig. 1e&f). Unlike macrophages, which shift their ratio of
156 succinate and α-ketoglutarate to favor succinate accumulation over α-ketoglutarate [29-31],
157 we found no changes in the levels of these metabolites in hepatocytes (Fig. 1G&H).
158 Furthermore, unlike macrophages [32], levels of fumarate decreased, but malate levels
159 were unchanged in hepatocytes from septic animals (Fig. 1I&J). Monocytes,
160 macrophages and dendritic cells reprogram the TCA cycle during acute inflammation to
161 a catabolic tolerance phenotype by shunting cis-aconitate to itaconate through the
162 enzymatic action of aconitase decarboxylase (ACOD1; also known as immune
163 responsive gene 1 [IRG1]) [32-35]. Accordingly, we also found that sepsis significantly
164 induces *ACOD1* and elevates itaconate in isolate hepatocyte preparations (Fig. 1K&L).
165

166 **Sepsis Impairs Hepatic Redox Balance and Promotes Oxidative Stress**

167 Perturbations in oxidative phosphorylation have been shown to promote the
168 production of reactive oxygen species (ROS) [36]. Furthermore, itaconate has been shown
169 to induce genes involved in oxidative stress regulation through activation of the master
170 NRF2 KEAP1 antioxidative pathway in macrophages [34]. Therefore, we examined if sepsis
171 invokes a gene expression profile involved in regulation of ROS. GSEA of the ROS
172 metabolic process pathway (GO:0072593) revealed a positive enrichment, highlighting

173 the transcriptional induction of genes involved in the regulation of oxidative stress in livers
174 of septic mice (Fig. 2a). Given the induction of ROS metabolic genes, we wanted to
175 determine if sepsis alters key metabolites involved in redox balance, specifically the
176 cysteine-glutathione transsulfuration redox regulatory cycle. Sepsis did not alter
177 intracellular homocysteine levels in isolated hepatocytes (Supplemental Fig. 1), however,
178 cystathionine decreased significantly (Fig. 2b). Furthermore, we found a trend for
179 decreased cysteine levels in the liver (p=0.0534) (Fig. 2c) and significantly decreased
180 glycine (Fig. 2d). Most dramatically, septic mice depleted hepatocyte glutathione (Fig. 2e)
181 and led to decreases in oxidized glutathione (GSSG) (Fig. 2f). Ophthalamate has recently
182 been shown to be a biomarker of oxidative stress and signals consumption of hepatic
183 GSH [37]. Functionally, we observe a significant accumulation of hepatic ophthalamate
184 levels in response to sepsis, signifying a state of oxidative injury (Fig. 2g).
185

186 **Sepsis promotes hepatic steatosis**

187 Thus far, our data has revealed that sepsis induces significant impairments in
188 hepatocyte OXPHOS, alterations in the TCA cycle, and induction of oxidative stress, find-
189 ings that are also metabolic hallmarks of fatty liver disease [38]. Because perturbations in
190 global lipid profiles occur in septic patients [15], we evaluated the effects of CLP on the
191 hepatic lipid metabolism pathway. In support of our hypothesis that sepsis alters hepatic
192 lipid metabolism, transcriptome data indicate significant repression of lipid metabolism in
193 livers of septic mice (Fig. 3a). Sepsis also decreased transcription output that supports
194 fatty acid metabolic process components in the liver, as evidenced by a negative GSEA

195 enrichment score (Fig. 3b). In particular, we find alterations in genes involved in both fatty
196 acid oxidation as well as fatty acid biosynthesis (Supplemental Fig. 2).

197 Since transcriptional regulation of hepatic lipid metabolism is significantly altered
198 during sepsis, we further investigated the functional manifestation of these gene expres-
199 sion profile. Consistent with our transcriptional profiling studies, our unbiased metabo-
200 lomic screening in hepatocytes also identified lipid metabolism as the top metabolic path-
201 way altered in sepsis (Fig.3c). We observe increases in virtually all fatty acids and acyl-
202 carnitine derivatives assayed (Fig. 3d). The dysregulation in hepatic lipid metabolism in
203 response to sepsis ultimately culminates in the development of steatosis, as evidenced
204 by increased free fatty acids, mono-, di- and triglycerides (Fig. 3e).

205

206 **Sepsis remodels the hepatic lipidome**

207 Given the severe dysregulation in hepatic lipid metabolism triggered by sepsis, we
208 next sought to characterize the global consequences on hepatic lipid profiles. This was
209 achieved by targeted lipidomic screening. Parallel to our unbiased metabolomic
210 screening, we find sepsis leads to profound accumulation of almost all lipid species
211 surveyed (Fig. 4a). We next evaluated the hepatic lipid composition to discern which lipid
212 species are must vulnerable to sepsis-induced alterations. We find very little alterations
213 to the ceramide pool in septic hepatocytes (Fig. 4b) with only modest changes in
214 dihydroceramide (Supplemental Fig 3.). However, the hepatic fatty acid fractions
215 displayed significant remodelling in response to sepsis (Fig. 4b). Specifically, we find
216 increases in free fatty acid species such as 16:0, 18:1 and 18:2 in septic hepatocytes
217 (Supplemental Fig. 4a). Morever, hepatic phospholipid composition showed robust

218 alterations following CLP (Fig. 4b). Of the phospholipids (PLs) most significantly affected,
219 we find accumulation of phosphotidylcholines (PCs), phosphotidylethanolamine (PE) and
220 sphingomyelin (SM) (Fig. 4c). Of the hepatic PC pool we find the most abundant species
221 (16:0/18:2 & 16:0/18:1) to show increased accumulion in response to sepsis
222 (Supplemental Fig. 4b). We also observed significant increases in the most abundant PE
223 species (18:0/20:4, 16:0/22:6 & 18:0/22:6) and SM species (22:0, 16:0 & 20:0) to show
224 significant accumulation in septic hepatocytes (Supplemental Fig. 4c&d). We did observe
225 a decrease in one phospholipid species, lysophosphatidylcholine, however, the hepatic
226 concentration of this phospholipid species is signifcantly lower than other PL species
227 assayed (Fig. 4c). Finally, we detected no differences in other PL species such as
228 phosphotidylinositol (PI) and lysophosphatidylethanolamine (LPE) and no differences in
229 hepatic cholesterol ester levels (Supplemental Fig. 5). Our data collectively detail the
230 impact of sepsis on hepatic lipid composition and robustly show a global rise in nearly all
231 lipid species.
232

233 **PDK inhibition attenuates sepsis-induced transcriptional and metabolic changes**
234 **in the liver**

235 We have previously reported that PDK inhibition by the pyruvate analog and pan-
236 PDK inhibitor dichloroacetate (DCA) promotes PDC-dependent immunometabolic adap-
237 tations to sepsis and increases survival [39]. Given the establishment of hepatocyte mito-
238 chondrial dysfunction and steatosis during sepsis, we asked whether pharmacological
239 targeting of the hepatic PDK/PDC axis would mitigate the disruption of key metabolic and
240 bioenergetic processes induced by sepsis. To test this postulate, we administered DCA

241 to septic mice 24 h after CLP onset and assessed the global transcription profile of liver
242 6 h later via RNA-seq. DCA treatment of septic mice reversed the majority of sepsis-
243 regulated gene networks (Fig. 5a). Most notably, pathways involved in redox homeosta-
244 sis, lipid metabolism and mitochondrial dysfunction are returned to control levels with the
245 administration of DCA in septic mice (Fig. 5b).

246 Given our previous results indicating the transcriptional changes associated with
247 sepsis in the liver underlie functional alterations in metabolism, we wanted to determine
248 if the DCA reversal of transcriptional changes mounts to differential metabolomes. Given
249 our RNA-seq data showing a positive enrichment score for production of ROS along with
250 negative enrichment for glutathione conjugation, we started off with evaluating the redox
251 pathway metabolites. Strikingly, the depletion of redox components cystathionine, cyste-
252 ine, glycine, hypotaurine, taurine and glutathione elicited by sepsis was completely re-
253 versed by administration of DCA (Fig. 5c). More importantly, we observed a significant
254 decrease in hepatic ophthalmate levels, signifying a functional decrease in oxidative
255 stress (Fig. 5c). The restoration in redox metabolites in septic mice following DCA admin-
256 istration prompted us to investigate the mitochondrial consequences of this pharmaco-
257 logical intervention. With the exception of fumarate, DCA completely restores TCA me-
258 tabolite levels to that of sham levels (Fig. 5d). Finally, we wished to define the effects of
259 DCA treatment on the hepatic lipidome. Lipidomic analysis shows a protective effect of
260 DCA in ameliorating sepsis-induced steatosis. In sum, these data reveal pharmacological
261 inhibition of the PDK pathway restores transcriptional and metabolic changes associated
262 with sepsis in the liver.

263

Discussion

Considerable attention has been focused recently on the immunometabolic consequences of inmflammation in immune cells [40]. However, significant gaps exist in our understanding of the metabolic adaptations induced by systeminc inflammation from sepsis in vital organs. Addressing this limitation is critical because sepsis survival depends on restoring both organ and immune cell homeostasis following dysregulated and disseminated inflammation [41]. In the present study, we reveal severe disruption of several key hepatic metabolic pathways in septic mice, including TCA cycle activity, OXPHOS, redox balance and lipid metabolism. Importantly, DCA administration restored TCA cycle flux, restored rerdox balance and ameliorated sepsis-induced steatosis. Our study highlights the clinical potential of targeting the PDC/PDK axis in restoring liver function/metabolism in the context of sepsis.

Remodelling of TCA cycle flux is well appreciated to support immune cell effector function in the face of inflammatory challenges [3,31,42,43]. For example, succinate primes inflammation through succinate dehydrogenase (SDH)-mediated ROS generation and ATP synthesis [31,42]. SDH-derived ROS enhances IL-1β production by activating HIF-1α and activating the NLRP3 inflammasome [20]. Inhibition of SDH activity increases IL-10 production and skews inflamed immune cells towards an anti-inflammatory response [31]. Fumarate, on the other hand, possesses anti-inflammatory properties as it inhibits pro-inflammatory cytokine production either by activating the NRF2 pathway or via inhibiting pathways like NF-κB and MAPK that lie downstream of TLR signaling in immune cells [44,45]. Our findings extend the concept that the TCA cycle is subject to reprogramming in response to sepsis in non-immune cells such as hepatocytes. Furthermore, we found

287 similarities as well as differences in terms of TCA cycle remodelling in hepatocytes com-
288 pared to immune cell effects, clearly indicating this pathway is regulated in a cell-type and
289 context-dependent manner during sepsis.

290 In response to LPS stimulation, macrophages significantly upregulate IRG1 and
291 accumulate itaconate from the decarboxylation of cis-aconitate [32,34]. One of the primary
292 functions itaconate serves in immune cells is to limit IL-1 β production through direct
293 inhibition of SDH and activation of the NRF2/Keap1 and IκBζ-ATF3 pathways [32,34,46]. In
294 line with what occurs in macrophages, we observed an increase in IRG1 and itaconate in
295 septic hepatocytes at 30h. While we did not fully characterize the hepatic function of
296 itaconate, a recent paper demonstrates its anti-inflammatory effects during Ischemia-
297 reperfusion (IR) injury in the liver [47]. The deletion of IRG1 heightens inflammation and
298 liver damage and renders hepatocytes susceptible to oxidative injury after I/R injury.
299 Further, itaconate administration reduces liver damage and inflammation associated with
300 I/R in IRG1 KO mice, also emphasizing its anti-inflammatory and hepatoprotective effects
301 [47]. Given the immunomodulatory effects of itaconate and its accumulation in the liver in
302 our study, we hypothesize that itaconate directs hepatocyte shifts in both TCA cycle
303 metabolism and mitochondrial energetics. DCA reduces itaconate levels, which we also
304 find in a human monocyte model of sepsis [48].

305 Similar to immune cells, liver cells increase ROS production during sepsis [49,50].
306 We offer a potential mechanism whereby sepsis leads to significant depletion of redox
307 metabolites within the glutathione pathway ultimately culminating in loss of cellular
308 glutathione levels resulting in ophthalamate accumulation in hepatocytes.

309 Sepsis profoundly alters lipid metabolism, resulting in significant increases in
310 plasma fatty acid and glycerol concentrations, changes reported to predict prognosis in
311 septic patients [51]. Furthermore, patients who died from sepsis had evidence of hepatic
312 steatosis affecting 5%-80% of liver parenchyma [52]. Human data supports a robust hepatic
313 steatosis phenotype subsequent to sepsis. One vital lipid metabolic pathway which can
314 contribute to steatosis is *de novo* lipogenesis. While we did not directly measure hepatic
315 lipogenesis, our metabolomics screening did show an increase in hepatic citrate and free
316 fatty acid levels suggesting an increased lipogenic drive during sepsis. Functionally,
317 immune cells exploit the lipogenic pathway for the generation of malonyl-CoA and
318 subsequent malonylation of glycolytic enzymes, which ultimately contributes to the
319 metabolic adaptation of macrophages to inflammatory cues [53]. Future studies dissecting
320 the role of lipogenesis in altering hepatocyte function during systemic infection are
321 warranted.

322 In addition to accumulation of free fatty acids and triglycerides in the liver, our
323 lipidomic analysis revealed significant increases in phospholipids. In the present study,
324 we find hepatic levels of the phospholipids phosphatidylcholine,
325 phosphatidylethanolamine, and sphingomyelin to be heightened during sepsis, indicating
326 abnormal metabolism of phospholipids. PC and PE are the most abundant phospholipids
327 that make up cellular membranes and an abnormally high ratio of PC and PE has been
328 reported to influence energy metabolsm and linked to fatty liver disease and impairement
329 in liver regeneration after injury [54-56]. Altered PC: PE ratio has also been shown to
330 influence the dynamics and regulation of lipid droplets contributing towards steatosis, a
331 phenotype we also report in our study [54,55,57]. The dysregulation of hepatic phospholipid

332 metabolism may be a contributing mechanism underlying steatosis, which is a topic of
333 future investigation. Additionally, phospholipids serve as precursor molecules to bioactive
334 lipids, which are involved in numerous signal transduction cascades [58]. Investigating
335 whether signaling properties of bioactive lipids in the liver during sepsis is pathogenic or
336 contributes to sepsis resolution is also needed in the future.

337 PDC is a master metabolic regulator controlling the conversion of pyruvate to
338 acetyl-CoA in the mitochondria [59] . A part of the metabolic reprogramming that occurs in
339 immune cells in response to inflammatory signaling is inactivation of PDC [22,59]. PDK is a
340 negative regulator of the PDC, as it phosphorylates PDC and inhibits the conversion of
341 pyruvate to acetyl-CoA [59]. During sepsis, the expression and activity of PDK1 in immune
342 cells is heightened, contributing to the dysfunction of mitochondria metabolism. One
343 mechanism driving this observed increase is through pro-inflammatory mediators such as
344 LPS and interferon gamma (IFN-γ) [60]. Another possible mechanism contributing to PDK
345 activation in the context of sepsis is through glucocorticoid signaling [61]. In fact, starvation
346 is well established to activate the PDK pathway [62-66]. Based on our findings of elevated
347 glucocorticoid levels in both the circulation and the liver, we hypothesize the stress
348 hormone pathway as a contributor to PDK activation during sepsis.

349 We reported in a sepsis monocyte model that DCA reduced TCA cycle catabolic
350 effects concurrent with increasing amino acid anaplerotic catabolism of branched-chain
351 amino acids, leading to increased TCA-driven anabolic energetics [22]. In the present
352 study, we find restoration of hepatic TCA metabolites, decreased triglyceride
353 accumulation, lessening of lipid synthesis and oxidative stress rebalances in septic mice

after DCA administration. Overall, we demonstrate that hepatic transcriptional and metabolic dysfunction improves after targeting the PDC/PDK axis with DCA.

Further work elucidating the mechanistic pathways involved in the dysfunction of lipid metabolism and the impact of TCA metabolite alterations is warranted. In particular, further investigation specifically into the PDK pathway to determine which isoform underlies the hepatic manifestions of sepsis. This is warranted given multiple isoforms of PDK expressed in the liver [67] and DCA inhibits multiple isoforms of PDK [68,69]. The results of this study fill a gap in understanding how sepsis at the molecular level compromises liver function. It also further informs the novel therapeutic targeting potential of the PDC/PDK homeostat.

Material and Methods

Animal Experiments

Male C57BL/6J mice aged 8-10 weeks were purchased from The Jackson Laboratory (Bar Harbor, ME). All animals were subject to a 12:12 hour dark/light cycle with *ad libitum* access to standard rodent chow and water. Cecal ligation puncture model was used to induce sepsis as previously described [39,70]. Briefly, cecum was ligated and punctured two times with a 22-gauge needle. Contents were then returned and incision was closed in two layers (peritoneum and skin). Sham operation where abdominal incision was made but cecum not ligated or punctured was used as a control. Subcutaneous fluids (1ml normal saline) were given to each animal. Mice were euthanized 30 hours post-surgery for tissue collection. Dichloroacetate (DCA) (Sigma; MO, USA) was administered (25mg/kg) intraperitoneally at various time points post-surgery: for metabolomic screening and RNA-seq DCA was administered 24 hours post-surgery and tissues collected 6 hours post DCA administration (30 hours post-surgery), for metabolic cages DCA was administered immediately post-surgery.

Hepatocyte Isolation

Hepatocytes were isolated via portal vein perfusion and collagenase digestion as previously described [71]. Following perfusion, liver cells were liberated by gentle dissocation in DMEM (ThermoFisher; CA, USA). Cells were then filtered through nylon mesh to remove cellular debris and connective tissue and resulting cells pelleted by centrifugation at 50g for 1 minute. After three washes with DMEM cells were counted and viability assessed via Trypan Blue exclusion.

403

404 **RNA-sequencing**

405 RNA was isolated from whole liver tissues using Trizol and the RNeasy RNA isolation kit
406 (Qiagen; MD, USA) according to manufacturer's protocol. One microgram of high quality
407 RNA (RIN>8) was used as a template for library generation using the Illumina TruSeq
408 RNA Sample Prep Kit v2 (Illumina; CA, USA) according to the manufacturer's protocol.
409 Generated libraries were then poly(A) enriched for mRNA prior to sequencing. Indexed
410 samples were sequenced at 100bp-paired-end protocol with the NovaSeq 6000
411 (Illumina), generating approximately 20-30 million reads per sample. Sequenced reads
412 were aligned to the University of California Santa Cruz (UCSC) mm10 reference genome
413 using STAR v2.5 as previously described [72]. The mapped read counts were quantified by
414 Subread feature Counts v1.5.0-p1 [73]. Differentially expressed genes (DEGs) were
415 determined by DESeq2 v1.14.1 [73] using a false discory rate of 0.05. Ingenuity Pathway
416 Analysis (Qiagen) and Gene Set Enrichment Analysis v4.0.3 (GSEA) were further used
417 as previously described [74].

418

419 **Ultrahigh Performance Liquid Chromatography-Tandem Mass Spectroscopy**

420 Hepatocytes were isolated described above for metabolomic screening via Ultrahigh
421 Performance Liquid Chromotography-Tandem Mass Spectroscopy (UPLC-MS/MS)
422 (Metabolon; NC, USA). Briefly, 150-200 microliter cell pellets per animal were used as
423 starting material. Samples were prepared using the automated MicroLab STAR system
424 (Hamilton; NV, USA). Proteins were precipitated using methanol under vigorous shaking
425 for 2 minutes followed by centrifugation. Prior to analysis organic solvents were removed

426 with TurboVap (Zymark; MA, USA) and overnight storage under nitrogen. Dried samples
427 were reconstituted with solvents compatible with the three following analytical methods:
428 1) reverse phase (RP)/UPLC-MS/MS methods with positive ion mode electrospray
429 ionization (ESI), 2) RP/UPLC-MS/MS with negative ion mode ESI and 3) HILIC/UPLC-
430 MS/MS with negative ion mode ESI. Resulting samples were analyzed with the ACQUITY
431 UPLC (Waters; MA, USA) and a Q-Exactive high resolution/accurate mass spectrometer
432 (ThermoScientific; MA, USA) interfaced with a heated electrospray ionization (HESI-II)
433 source and Orbitrap mass analyzer operated at 35,000 mass resolution. An acidic positive
434 ion condition was used on an aliquot optimized to detect more hydrophilic compounds.
435 Another acidic positive ion condition was ran but chromotographically optimized for
436 hydrophobic compounds. Basic negative ion optimized conditions was also used on a
437 separate C18 column. Resulting raw data was extracted and peaks identified using
438 Metabolon's hardware and software. Compounds were identified by comnparing to known
439 library entries of purified standards or recurrent unknown entities. A lirary of authenticated
440 standards containing retention time/index (RI), mass to charge ratio (*m/z*) and
441 chromotographic data (MS/MS spectral data) on all library compounds. Three criteria are
442 used to identify chemicals: 1) RI within a narrow window of proposed identification, 2)
443 accurate mass match to the library ± 10 ppm and 3) MS/MS forward and reverse scores
444 between the experimental data and authentic standards. Peaks were quantified using
445 area under the curve (AUC). For complex lipid panel lipids were extracted with
446 methanol:dichloromethane in the presence of internal standards. Extracts were
447 concentrated under nitrogen and reconstituted in 250ml of 10mM ammonium acetate
448 dichloromethane:methanol (50:50). Mass spec analysis was performed in a Shimazdu LC

with nano PEEK tubing and the Sciex SlexIon-5500 QTRAP (Sciex; MA, USA). Both negative and positive mode electrospray was used. Individual lipid species were quantified by taking the peak area ratios of target compounds and their assigned internal standards then multiplying by the concentration of added internal standards. Lipid class concentrations were calculated from the sum of all molecular species within a class, and fatty acid compositions were determined by calculating the proportion of each class comprised by individual fatty acids.

Acknowledgements

The authors of this manuscript would like to thank the National Institute of Environmental Health Sciences Epigenomics and DNA Sequencing Core for their help with RNA-sequencing and Dr. Sara Grimm for her analysis of transcriptome data. This work was supported by NIH Intramural Program 1ZIAES10328601 (J.M.), NIH R01 HL132035 (X.Z.), NIH R01 HL119962 (J.S.P.), NIH K01 DK117069 (C.K), NIH K01 AG056663 (E.Q.), NIH R01 AI065791 (C.E.M.), R01 GM102497 (C.E.M.), R35 GM126922 (C.E.M.).

Citations

480 1 Lewis, A. J., Billiar, T. R. & Rosengart, M. R. Biology and metabolism of sepsis: innate immunity,
481 bioenergetics, and autophagy. *Surgical infections* **17**, 286-293 (2016).
482 2 Bermudes, A. C. G. *et al.* Changes in lipid metabolism in pediatric patients with severe sepsis and
483 septic shock. *Nutrition* **47**, 104-109 (2018).
484 3 Cheng, S.-C. *et al.* Broad defects in the energy metabolism of leukocytes underlie
485 immunoparalysis in sepsis. *Nature immunology* **17**, 406 (2016).
486 4 Levi, M. & van der Poll, T. Coagulation and sepsis. *Thrombosis research* **149**, 38-44 (2017).
487 5 Schneck, E. *et al.* Plasma DNA and RNA differentially impact coagulation during abdominal
488 sepsis—an explorative study. *Journal of Surgical Research* **210**, 231-243 (2017).
489 6 McDonald, B. *et al.* Platelets and neutrophil extracellular traps collaborate to promote
490 intravascular coagulation during sepsis in mice. *Blood, The Journal of the American Society of*
491 *Hematology* **129**, 1357-1367 (2017).
492 7 Kidokoro, A., Iba, T., Fukunaga, M. & Yagi, Y. Alterations in coagulation and fibrinolysis during
493 sepsis. *Shock (Augusta, Ga.)* **5**, 223-228 (1996).
494 8 Rhee, C. *et al.* Incidence and trends of sepsis in US hospitals using clinical vs claims data, 2009-
495 2014. *Jama* **318**, 1241-1249 (2017).
496 9 Buchman, T. G. *et al.* Sepsis Among Medicare Beneficiaries: 1. The Burdens of Sepsis, 2012–
497 2018. *Critical Care Medicine* **48**, 276 (2020).
498 10 Osuchowski, M. F., Craciun, F., Weixelbaumer, K. M., Duffy, E. R. & Remick, D. G. Sepsis
499 chronically in MARS: systemic cytokine responses are always mixed regardless of the outcome,
500 magnitude, or phase of sepsis. *The Journal of Immunology* **189**, 4648-4656 (2012).
501 11 Chiswick, E. L., Mella, J. R., Bernardo, J. & Remick, D. G. Acute-phase deaths from murine
502 polymicrobial sepsis are characterized by innate immune suppression rather than exhaustion.
503 *The Journal of Immunology* **195**, 3793-3802 (2015).
504 12 Xiao, H., Siddiqui, J. & Remick, D. G. Mechanisms of mortality in early and late sepsis. *Infection*
505 *and immunity* **74**, 5227-5235 (2006).
506 13 Singer, M. The role of mitochondrial dysfunction in sepsis-induced multi-organ failure. *Virulence*
507 **5**, 66-72 (2014).
508 14 Druml, W., Heinzel, G. & Kleinberger, G. Amino acid kinetics in patients with sepsis. *The*
509 *American journal of clinical nutrition* **73**, 908-913 (2001).
510 15 Mecatti, G. C., Messias, M. C. F. & de Oliveira Carvalho, P. Lipidomic profile and candidate
511 biomarkers in septic patients. *Lipids in Health and Disease* **19**, 1-9 (2020).
512 16 Seymour, C. W. *et al.* Metabolomics in pneumonia and sepsis: an analysis of the GenIMS cohort
513 study. *Intensive care medicine* **39**, 1423-1434 (2013).
514 17 Quinones, Q. J., Ma, Q., Zhang, Z., Barnes, B. M. & Podgoreanu, M. V. Organ protective
515 mechanisms common to extremes of physiology: a window through hibernation biology.
516 *American Zoologist* **54**, 497-515 (2014).
517 18 Singer, M., De Santis, V., Vitale, D. & Jeffcoate, W. Multiorgan failure is an adaptive, endocrine-
518 mediated, metabolic response to overwhelming systemic inflammation. *The Lancet* **364**, 545-
519 548 (2004).
520 19 McCall, C. E. *et al.* Pyruvate dehydrogenase complex stimulation promotes immunometabolic
521 homeostasis and sepsis survival. *JCI insight* **3** (2018).
522 20 Vary, T. C. Increased pyruvate dehydrogenase kinase activity in response to sepsis. *American*
523 *Journal of Physiology-Endocrinology and Metabolism* **260**, E669-E674 (1991).
524 21 Stacpoole, P. W. The pharmacology of dichloroacetate. *Metabolism* **38**, 1124-1144 (1989).
525 22 Zhu, X. *et al.* Stimulating pyruvate dehydrogenase complex reduces itaconate levels and
526 enhances TCA cycle anabolic bioenergetics in acutely inflamed monocytes. *Journal of Leukocyte*
527 *Biology* (2020).

528 23 Kelly, B. & O'neill, L. A. Metabolic reprogramming in macrophages and dendritic cells in innate
529 immunity. *Cell research* **25**, 771-784 (2015).
530 24 Eyenga, P. *et al.* Time course of liver mitochondrial function and intrinsic changes in oxidative
531 phosphorylation in a rat model of sepsis. *Intensive care medicine experimental* **6**, 31 (2018).
532 25 Ilaiwy, A. *et al.* Identification of Metabolic Changes in Ileum, Jejunum, Skeletal Muscle, Liver, and
533 Lung in a Continuous IV Pseudomonas aeruginosa Model of Sepsis Using Nontargeted
534 Metabolomics Analysis. *The American journal of pathology* **189**, 1797-1813 (2019).
535 26 Dahn, M. S., Mitchell, R. A., Lange, M. P., Smith, S. & Jacobs, L. A. Hepatic metabolic response to
536 injury and sepsis. *Surgery* **117**, 520-530 (1995).
537 27 Levy, E., Slusser, R. J. & Ruebner, B. Hepatic changes produced by a single dose of endotoxin in
538 the mouse. Electron microscopy. *The American journal of pathology* **52**, 477 (1968).
539 28 Han, X., Fink, M. P., Uchiyama, T., Yang, R. & Delude, R. L. Increased iNOS activity is essential for
540 hepatic epithelial tight junction dysfunction in endotoxemic mice. *American Journal of*
541 *Physiology-Gastrointestinal and Liver Physiology* **286**, G126-G136 (2004).
542 29 Liu, P. S. *et al.* alpha-ketoglutarate orchestrates macrophage activation through metabolic and
543 epigenetic reprogramming. *Nat Immunol* **18**, 985-994, doi:10.1038/ni.3796 (2017).
544 30 Mills, E. & O'Neill, L. A. Succinate: a metabolic signal in inflammation. *Trends Cell Biol* **24**, 313-
545 320, doi:10.1016/j.tcb.2013.11.008 (2014).
546 31 Mills, E. L. *et al.* Succinate Dehydrogenase Supports Metabolic Repurposing of Mitochondria to
547 Drive Inflammatory Macrophages. *Cell* **167**, 457-470 e413, doi:10.1016/j.cell.2016.08.064
548 (2016).
549 32 Lampropoulou, V. *et al.* Itaconate Links Inhibition of Succinate Dehydrogenase with Macrophage
550 Metabolic Remodeling and Regulation of Inflammation. *Cell Metab* **24**, 158-166,
551 doi:10.1016/j.cmet.2016.06.004 (2016).
552 33 Liao, S. T. *et al.* 4-Octyl itaconate inhibits aerobic glycolysis by targeting GAPDH to exert anti-
553 inflammatory effects. *Nat Commun* **10**, 5091, doi:10.1038/s41467-019-13078-5 (2019).
554 34 Mills, E. L. *et al.* Itaconate is an anti-inflammatory metabolite that activates Nrf2 via alkylation of
555 KEAP1. *Nature* **556**, 113-117, doi:10.1038/nature25986 (2018).
556 35 Daniels, B. P. *et al.* The Nucleotide Sensor ZBP1 and Kinase RIPK3 Induce the Enzyme IRG1 to
557 Promote an Antiviral Metabolic State in Neurons. *Immunity* **50**, 64-76 e64,
558 doi:10.1016/j.immuni.2018.11.017 (2019).
559 36 Indo, H. P. *et al.* Evidence of ROS generation by mitochondria in cells with impaired electron
560 transport chain and mitochondrial DNA damage. *Mitochondrion* **7**, 106-118,
561 doi:10.1016/j.mito.2006.11.026 (2007).
562 37 Soga, T. *et al.* Differential metabolomics reveals ophthalmic acid as an oxidative stress
563 biomarker indicating hepatic glutathione consumption. *J Biol Chem* **281**, 16768-16776,
564 doi:10.1074/jbc.M601876200 (2006).
565 38 Simoes, I. C. M., Fontes, A., Pinton, P., Zischka, H. & Wieckowski, M. R. Mitochondria in non-
566 alcoholic fatty liver disease. *Int J Biochem Cell Biol* **95**, 93-99, doi:10.1016/j.biocel.2017.12.019
567 (2018).
568 39 McCall, C. E. *et al.* Pyruvate dehydrogenase complex stimulation promotes immunometabolic
569 homeostasis and sepsis survival. *JCI Insight* **3**, doi:10.1172/jci.insight.99292 (2018).
570 40 Buck, M. D., Sowell, R. T., Kaech, S. M. & Pearce, E. L. Metabolic Instruction of Immunity. *Cell*
571 **169**, 570-586, doi:10.1016/j.cell.2017.04.004 (2017).
572 41 Singer, M. *et al.* The Third International Consensus Definitions for Sepsis and Septic Shock
573 (Sepsis-3). *JAMA* **315**, 801-810, doi:10.1001/jama.2016.0287 (2016).
574 42 Williams, N. C. & O'Neill, L. A. A role for the Krebs cycle intermediate citrate in metabolic
575 reprogramming in innate immunity and inflammation. *Frontiers in immunology* **9**, 141 (2018).

576 43 Zaslona, Z. & O'Neill, L. A. J. Cytokine-like Roles for Metabolites in Immunity. *Mol Cell*,
577 doi:10.1016/j.molcel.2020.04.002 (2020).
578 44 McGuire, V. A. *et al.* Dimethyl fumarate blocks pro-inflammatory cytokine production via
579 inhibition of TLR induced M1 and K63 ubiquitin chain formation. *Scientific reports* **6**, 31159
580 (2016).
581 45 Della Giustina, A. *et al.* Dimethyl fumarate modulates oxidative stress and inflammation in
582 organs after Sepsis in rats. *Inflammation* **41**, 315-327 (2018).
583 46 Bambouskova, M. *et al.* Electrophilic properties of itaconate and derivatives regulate the
584 IkappaBzeta-ATF3 inflammatory axis. *Nature* **556**, 501-504, doi:10.1038/s41586-018-0052-z
585 (2018).
586 47 Yi, Z. *et al.* IRG1/Itaconate Activates Nrf2 in Hepatocytes to Protect Against Liver Ischemia-
587 Reperfusion Injury. *Hepatology*, doi:10.1002/hep.31147 (2020).
588 48 Zhu, X. *et al.* Stimulating pyruvate dehydrogenase complex reduces itaconate levels and
589 enhances TCA cycle anabolic bioenergetics in acutely inflamed monocytes. *J Leukoc Biol* **107**,
590 467-484, doi:10.1002/JLB.3A1119-236R (2020).
591 49 Giustina, A. D. *et al.* Vitamin B6 reduces oxidative stress in lungs and liver in experimental sepsis.
592 *An Acad Bras Cienc* **91**, e20190434, doi:10.1590/0001-3765201920190434 (2019).
593 50 Chen, J. *et al.* Protective effects of melatonin on sepsis-induced liver injury and dysregulation of
594 gluconeogenesis in rats through activating SIRT1/STAT3 pathway. *Biomed Pharmacother* **117**,
595 109150, doi:10.1016/j.biopha.2019.109150 (2019).
596 51 Langley, R. J. *et al.* An integrated clinico-metabolomic model improves prediction of death in
597 sepsis. *Sci Transl Med* **5**, 195ra195, doi:10.1126/scitranslmed.3005893 (2013).
598 52 Koskinas, J. *et al.* Liver histology in ICU patients dying from sepsis: a clinico-pathological study.
599 *World journal of gastroenterology: WJG* **14**, 1389 (2008).
600 53 Galvan-Pena, S. *et al.* Malonylation of GAPDH is an inflammatory signal in macrophages. *Nat*
601 *Commun* **10**, 338, doi:10.1038/s41467-018-08187-6 (2019).
602 54 van der Veen, J. N. *et al.* (Elsevier, 2017).
603 55 Ling, J., Chaba, T., Zhu, L. F., Jacobs, R. L. & Vance, D. E. Hepatic ratio of phosphatidylcholine to
604 phosphatidylethanolamine predicts survival after partial hepatectomy in mice. *Hepatology* **55**,
605 1094-1102 (2012).
606 56 Li, Z. *et al.* The ratio of phosphatidylcholine to phosphatidylethanolamine influences membrane
607 integrity and steatohepatitis. *Cell metabolism* **3**, 321-331 (2006).
608 57 Listenberger, L. *et al.* Decreasing phosphatidylcholine on the surface of the lipid droplet
609 correlates with altered protein binding and steatosis. *Cells* **7**, 230 (2018).
610 58 Sunshine, H. & Iruela-Arispe, M. L. Membrane lipids and cell signaling. *Current opinion in*
611 *lipidology* **28**, 408 (2017).
612 59 Stacpoole, P. W. The pyruvate dehydrogenase complex as a therapeutic target for age-related
613 diseases. *Aging cell* **11**, 371-377 (2012).
614 60 Min, B. K. *et al.* Pyruvate Dehydrogenase Kinase Is a Metabolic Checkpoint for Polarization of
615 Macrophages to the M1 Phenotype. *Front Immunol* **10**, 944, doi:10.3389/fimmu.2019.00944
616 (2019).
617 61 Huang, B., Wu, P., Bowker-Kinley, M. M. & Harris, R. A. Regulation of pyruvate dehydrogenase
618 kinase expression by peroxisome proliferator-activated receptor-alpha ligands, glucocorticoids,
619 and insulin. *Diabetes* **51**, 276-283, doi:10.2337/diabetes.51.2.276 (2002).
620 62 Hutson, N. J. & Randle, P. J. Enhanced activity of pyruvate dehydrogenase kinase in rat heart
621 mitochondria in alloxan-diabetes or starvation. *FEBS Lett* **92**, 73-76, doi:10.1016/0014-
622 5793(78)80724-8 (1978).

63 Baxter, M. A. & Coore, H. G. The mode of regulation of pyruvate dehydrogenase of lactating rat mammary gland. Effects of starvation and insulin. *Biochem J* **174**, 553-561, doi:10.1042/bj1740553 (1978).

64 Fuller, S. J. & Randle, P. J. Reversible phosphorylation of pyruvate dehydrogenase in rat skeletal-muscle mitochondria. Effects of starvation and diabetes. *Biochem J* **219**, 635-646, doi:10.1042/bj2190635 (1984).

65 Denyer, G. S., Kerbey, A. L. & Randle, P. J. Kinase activator protein mediates longer-term effects of starvation on activity of pyruvate dehydrogenase kinase in rat liver mitochondria. *Biochem J* **239**, 347-354, doi:10.1042/bj2390347 (1986).

66 Wu, P. *et al.* Starvation increases the amount of pyruvate dehydrogenase kinase in several mammalian tissues. *Arch Biochem Biophys* **381**, 1-7, doi:10.1006/abbi.2000.1946 (2000).

67 Klyuyeva, A., Tuganova, A., Kedishvili, N. & Popov, K. M. Tissue-specific kinase expression and activity regulate flux through the pyruvate dehydrogenase complex. *J Biol Chem* **294**, 838-851, doi:10.1074/jbc.RA118.006433 (2019).

68 Bao, H., Kasten, S. A., Yan, X. & Roche, T. E. Pyruvate dehydrogenase kinase isoform 2 activity limited and further inhibited by slowing down the rate of dissociation of ADP. *Biochemistry* **43**, 13432-13441, doi:10.1021/bi049488x (2004).

69 Pratt, M. L. & Roche, T. E. Mechanism of pyruvate inhibition of kidney pyruvate dehydrogenasea kinase and synergistic inhibition by pyruvate and ADP. *J Biol Chem* **254**, 7191-7196 (1979).

70 Vachharajani, V. T. *et al.* SIRT1 inhibition during the hypoinflammatory phenotype of sepsis enhances immunity and improves outcome. *J Leukoc Biol* **96**, 785-796, doi:10.1189/jlb.3MA0114-034RR (2014).

71 Chen, Z., Fitzgerald, R. L., Averna, M. R. & Schonfeld, G. A targeted apolipoprotein B-38.9-producing mutation causes fatty livers in mice due to the reduced ability of apolipoprotein B-38.9 to transport triglycerides. *J Biol Chem* **275**, 32807-32815, doi:10.1074/jbc.M004913200 (2000).

72 Dobin, A. *et al.* STAR: ultrafast universal RNA-seq aligner. *Bioinformatics* **29**, 15-21, doi:10.1093/bioinformatics/bts635 (2013).

73 Liao, Y., Smyth, G. K. & Shi, W. featureCounts: an efficient general purpose program for assigning sequence reads to genomic features. *Bioinformatics* **30**, 923-930, doi:10.1093/bioinformatics/btt656 (2014).

74 Quinn, M. A., Xu, X., Ronfani, M. & Cidlowski, J. A. Estrogen Deficiency Promotes Hepatic Steatosis via a Glucocorticoid Receptor-Dependent Mechanism in Mice. *Cell Rep* **22**, 2690-2701, doi:10.1016/j.celrep.2018.02.041 (2018).

Figure Legends

662 **Figure 1: Sepsis Impairs hepatic mitochondrial metabolism.** (A) Top 5 canonical
663 pathways subject to transcriptional alterations in the liver identified by Ingenuity Pathway
664 Analysis of RNA-seq of sham versus CLP mice (n = 4 mice per group). Blue represents
665 a negative z-score and orange represents a positive z-score. Shading indicates intensity
666 of pathway activation/inhibition. (B) GSEA of the oxidative phosphorylation pathway
667 (GO:0006119) indicating a negative normalized enrichment score (NES = -0.853). (C)
668 GSEA of the TCA cycle pathway (GO:0006099) indicating a negative enrichment score
669 (NES = -1.1956). (D) Schematic representation of hepatic TCA cycle metabolites altered
670 during chronic sepsis. Red denotes a metabolite increased in response to sepsis; green
671 indicates a metabolite decreased in response to sepsis; black indicates a metabolite un-
672 changed in response to sepsis; grey indicates a metabolite not measured in our metabo-
673 lomic screening. (E-J) Relative metabolite levels measured by Ultrahigh Performance Liq-
674 uid Chromatography-Tandem Mass Spectroscopy (UPLC-MS/MS) from livers of sham
675 and CLP mice 30 hours post-surgery (n = 5 sham; 8 CLP). (K) rlog transformed counts
676 from RNA-seq of sham and CLP mice 30 hours post-surgery. (L) Relative itaconate levels
677 in livers of sham and CLP mice measured by UPLC-MS/MS (n = 5 sham; 8 CLP). * de-
678 notes $p<0.05$.

679

680 **Figure 2: Impaired hepatic redox balance in septic mice.** (A) GSEA of the ROS met-
681 abolic pathway (GO:0072593) from RNA-seq from livers comparing sham to CLP showing
682 a positive enrichment score (NES = 1.117) (n = 4 mice per group). (B-F) Relative metab-
683 olite levels of metabolites involved in redox balance measured by UPLC-MS/MS (n = 5

684 sham; 8 CLP). (G) Relative levels of ophthalmate involved in redox balance measured by
685 UPLC-MS/MS. * denotes p<0.05, ** p<0.01, **** p<0.0001.

686

687 **Figure 3: Sepsis promotes hepatic steatosis.** (A) Top 5 induced and repressed physi-
688 ological pathways in the liver of sham versus CLP mice identified by IPA of RNA-seq. (B)
689 GSEA of the fatty acid metabolic pathway (GO:0019395) from RNA-seq from livers com-
690 paring sham to CLP showing a negative enrichment score (NES = -1.018) (n = 4 mice per
691 group). (C) IPA of top 5 metabolic pathways significantly altered in the liver in response
692 to sepsis identified by global metabolomic screening. (D) Heatmap representation of log2
693 fold change of different lipid species in sham and CLP mice measured by UPLC-MS/MS.
694 (E) Quantification of lipids by UPLC-MS/MS in hepatocytes isolated from sham and CLP
695 mice 30 hours post-surgery (n = 5 sham; n = 8 CLP). * denotes p<0.05, ** p<0.01, ***
696 p<0.001.

697

698 **Figure 4: Sepsis reprograms the hepatic lipidome.** (A) Volcano plot of significantly
699 altered lipids from sham and CLP hepatocytes measured by UPLC-MS/MS (n = 5 sham;
700 n = 8 CLP). (B) Pie chart of lipid compositions from sham and CLP mice. (C) Quantifica-
701 tion of lipids by UPLC-MS/MS in hepatocytes isolated from sham and CLP mice 30 hours
702 post-surgery (n = 5 sham; n = 8 CLP). ** denotes p<0.01, *** p<0.001, **** p<0.0001.

703

704 **Figure 5: PDK inhibition restores hepatic metabolism in septic mice.** (A) Venn dia-
705 gram of differentially expressed genes (DEGs) assessed by RNA-seq in CLP versus

706 sham compared to CLP+DCA versus sham 30 hours post-surgery (left). Heatmap of av-
707 erage log2 fold change of DEGs in sham, CLP and CLP+DCA (right) (n = 4 mice per
708 group). (B) Heatmap depiction of z-scores of top canonical pathways identified by IPA in
709 CLP versus sham and CLP+DCA versus sham. (C) Heatmap depiction of average log2
710 fold change in metabolite levels involved in redox balance in sham, CLP and CLP+DCA
711 24 hours post-surgery measured by UPLC-MS/MS (n = 5 sham; n = 8 CLP and
712 CLP+DCA). (D) Heatmap depiction of average log2 fold change in metabolite levels in-
713 volved in TCA cycle in sham, CLP and CLP+DCA 30 hours post-surgery measured by
714 UPLC-MS/MS (n = 5 sham; n = 8 CLP and CLP+DCA). (E) Heatmap depiction of average
715 log2 fold change in MAG, DAG and TAG levels in sham, CLP and CLP+DCA 30 hours
716 post-surgery measured by UPLC-MS/MS (n = 5 sham; n = 8 CLP and CLP+DCA). (F)
717 Heatmap depiction of average log2 fold change in phospholipids in sham, CLP and
718 CLP+DCA 30 hours post-surgery measured by UPLC-MS/MS (n = 5 sham; n = 8 CLP
719 and CLP+DCA.

720

721

722

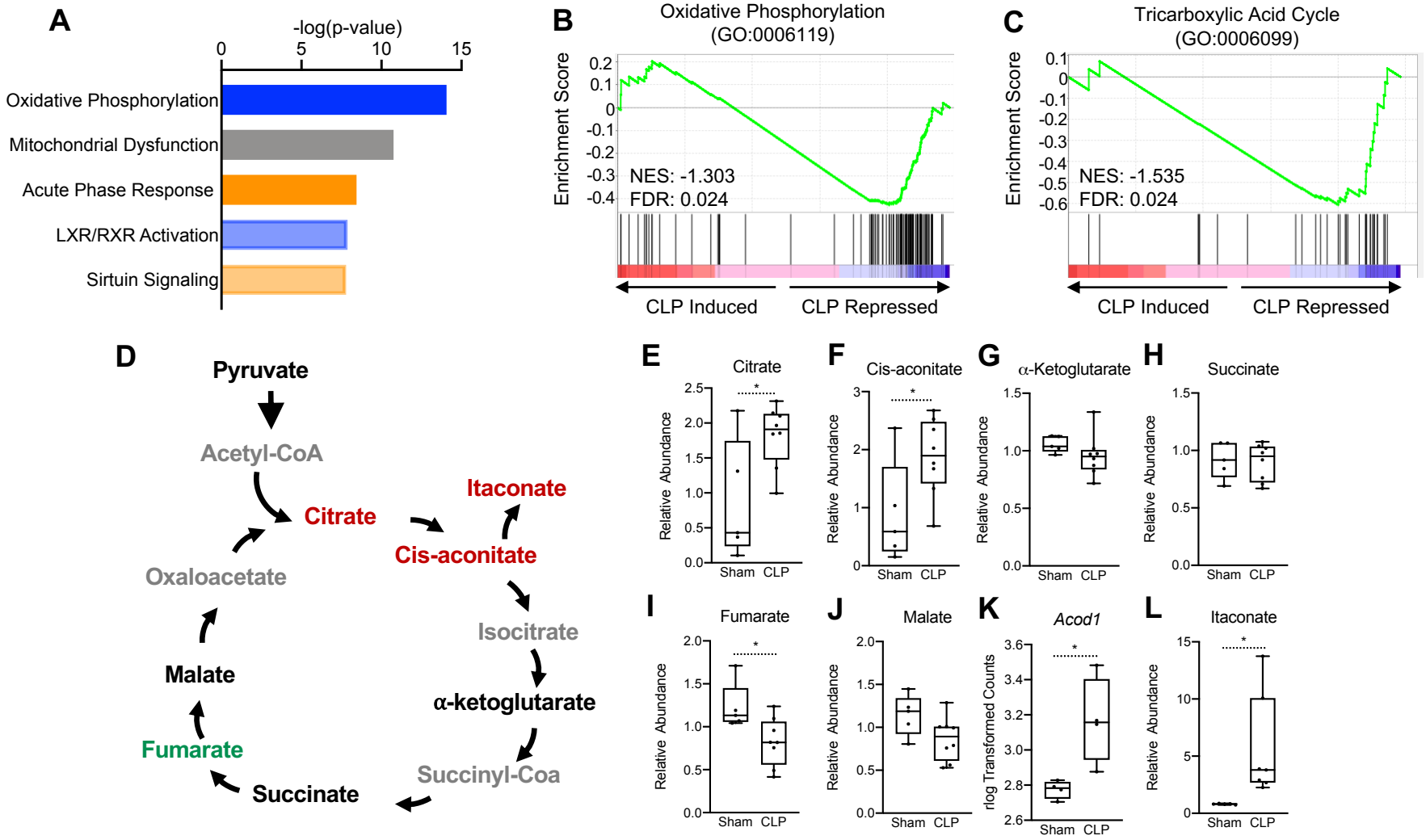

Figure 1: Sepsis Impairs Hepatic Mitochondrial Metabolism

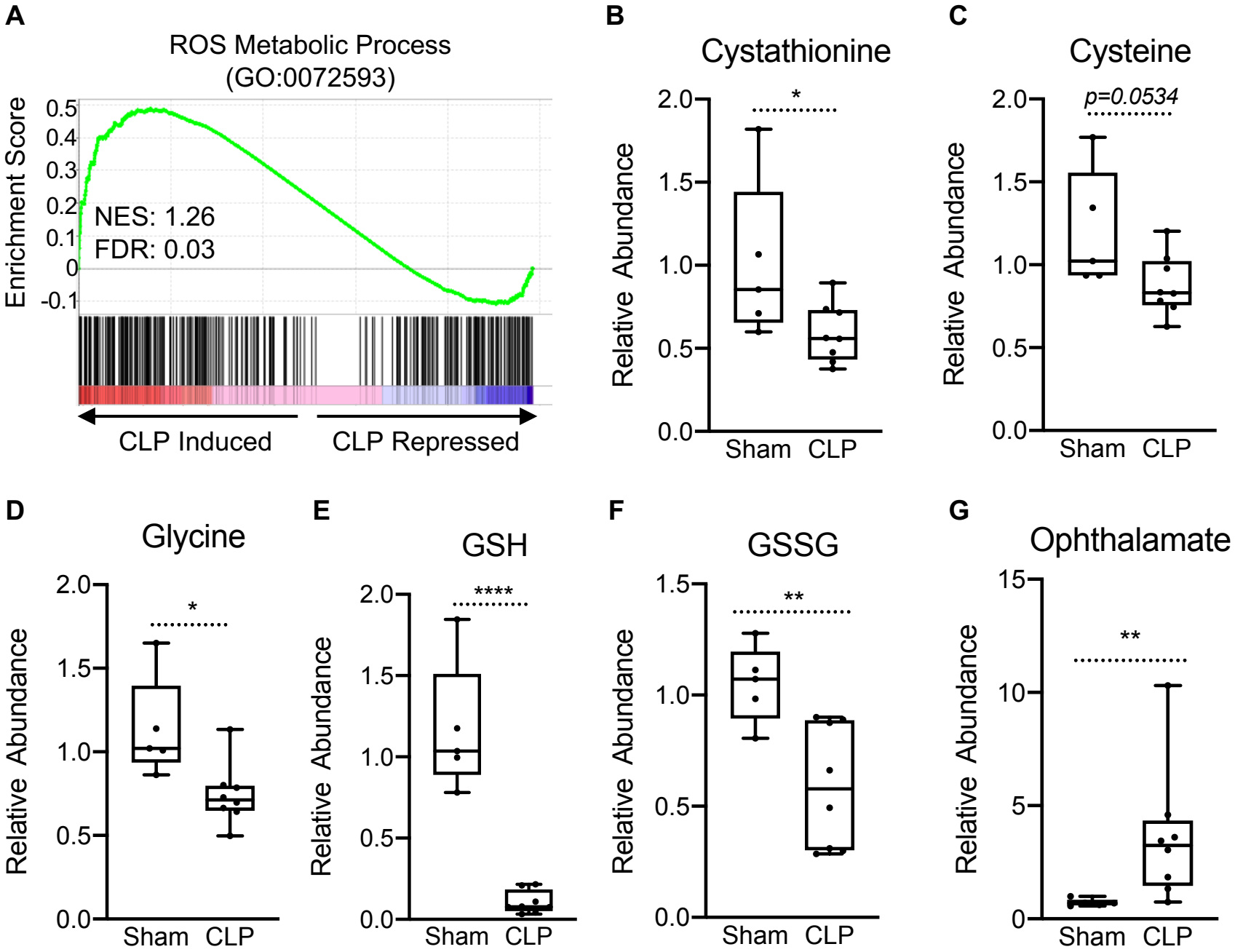

Figure 2: Impaired Hepatic Redox Balance in Septic Mice

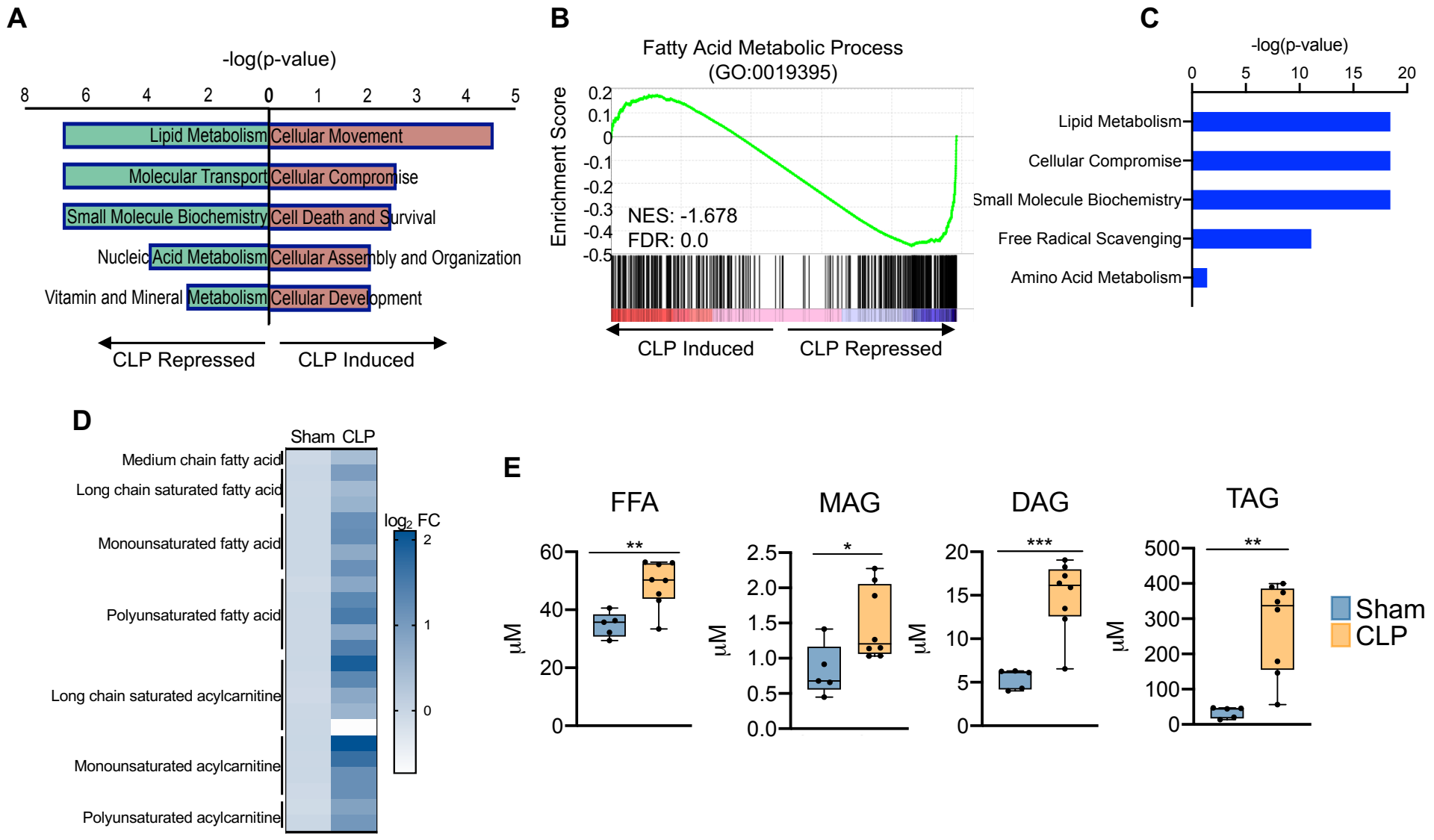

Figure 3: Sepsis promotes hepatic steatosis

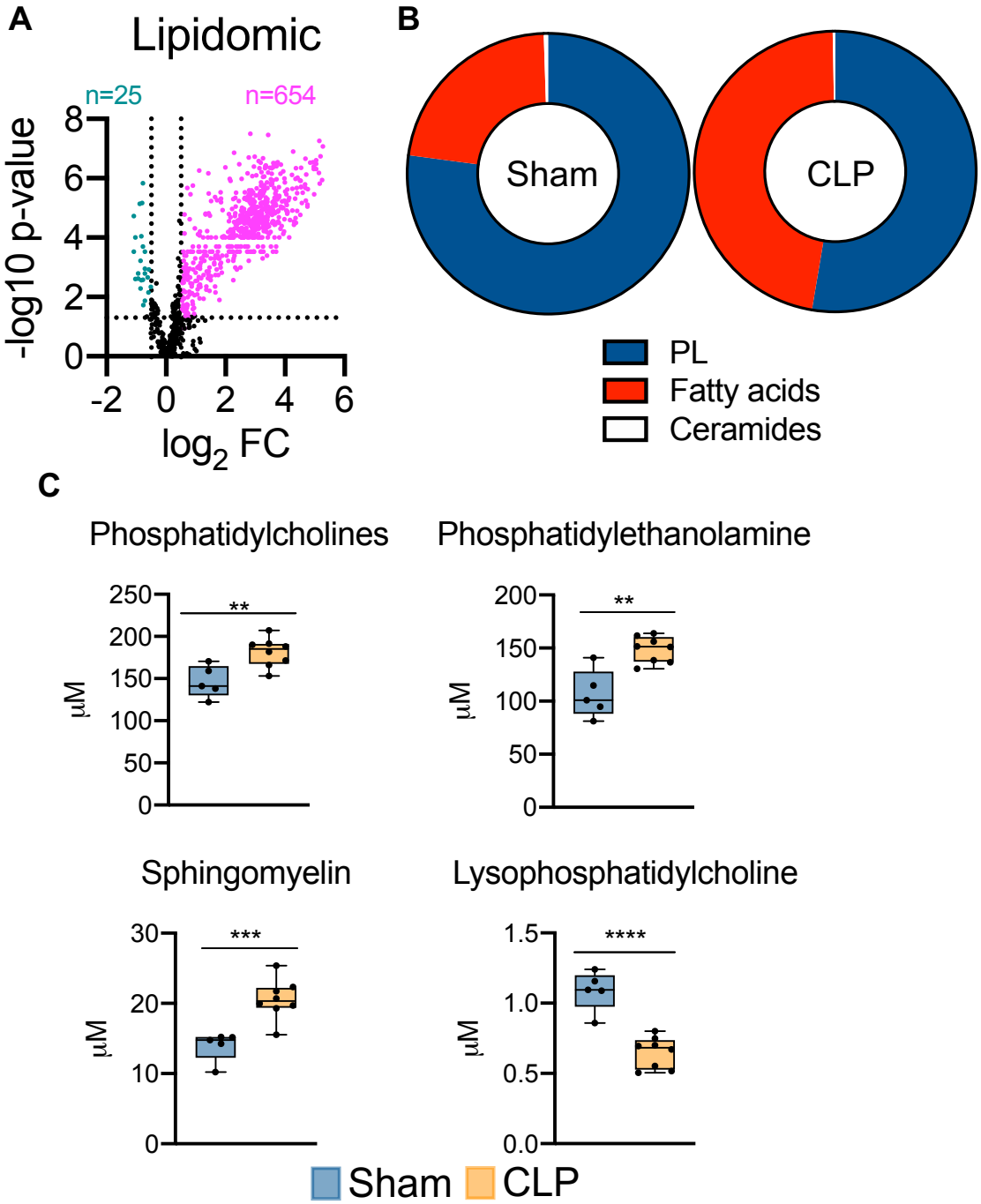

Figure 4: Sepsis reprograms the hepatic lipidome

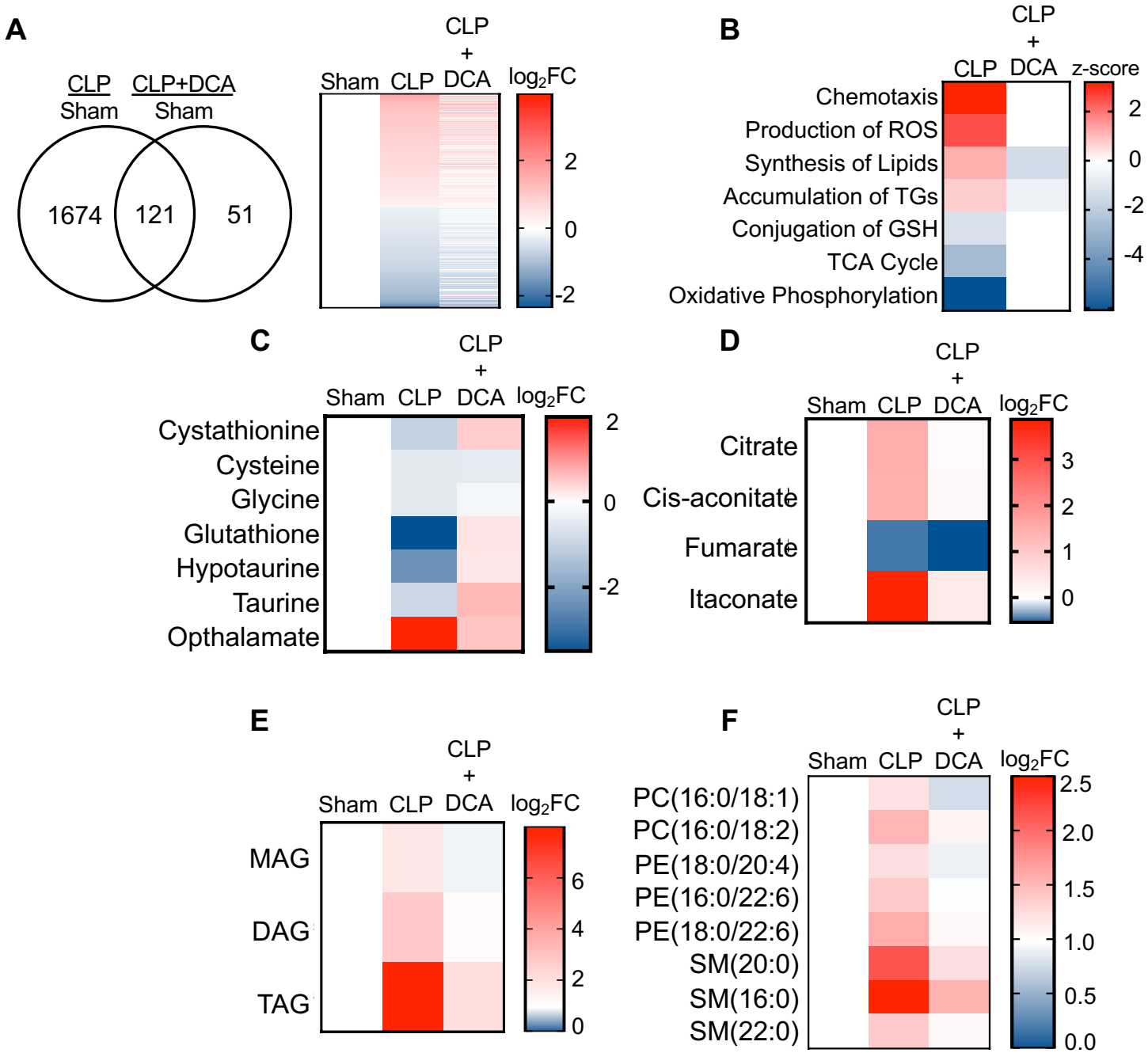

Figure 5: DCA reverses transcriptional and metabolic changes elicited by sepsis in the liver

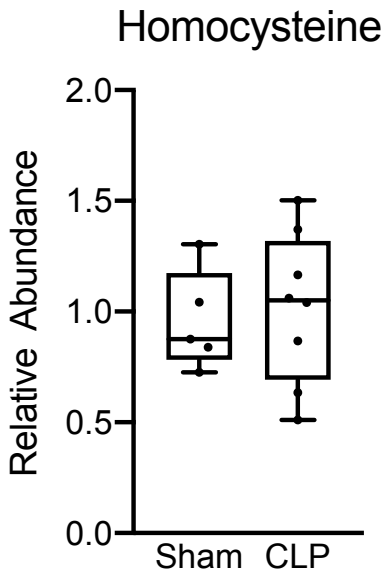

Supplemental figure 1: Hepatic homocysteine levels in sham and CLP mice. Ultrahigh Performance Liquid Chromatography-Tandem Mass Spectroscopy measurement of homocysteine from isolated hepatocytes 30 hours post-surgery. n=5 sham, n=8 CLP.

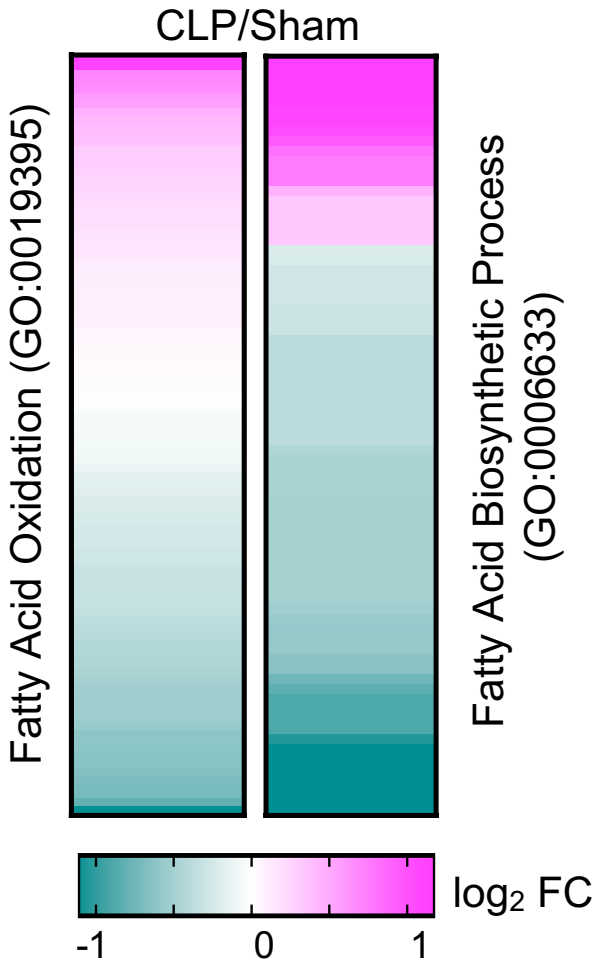

Supplemental figure 2: Fatty acid oxidation and biosynthetic pathways in septic livers. Heatmap representation of average log2 fold change of genes involved in fatty acid oxidation (GO:0019395) and fatty acid biosynthetic process (GO:0006633) in CLP versus sham operated mice (n = 5 sham; n = 8 CLP).

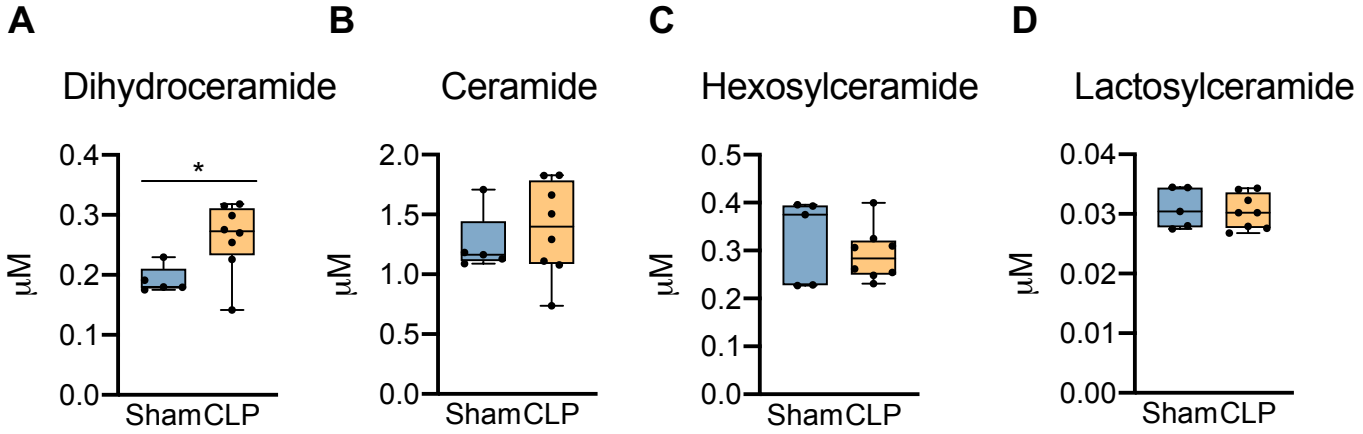

Supplemental figure 3: Hepatic ceramide levels in sham and CLP mice. Ultrahigh Performance Liquid Chromatography-Tandem Mass Spectroscopy measurement of **(A)** dihydroceramide, **(B)** ceramide, **(C)** hexosylceramide and **(D)** lactosylceramide from isolated hepatocytes 30 hours post-surgery. n=5 sham, n=8 CLP. * denotes $p<0.05$ determined by Student's T-test.

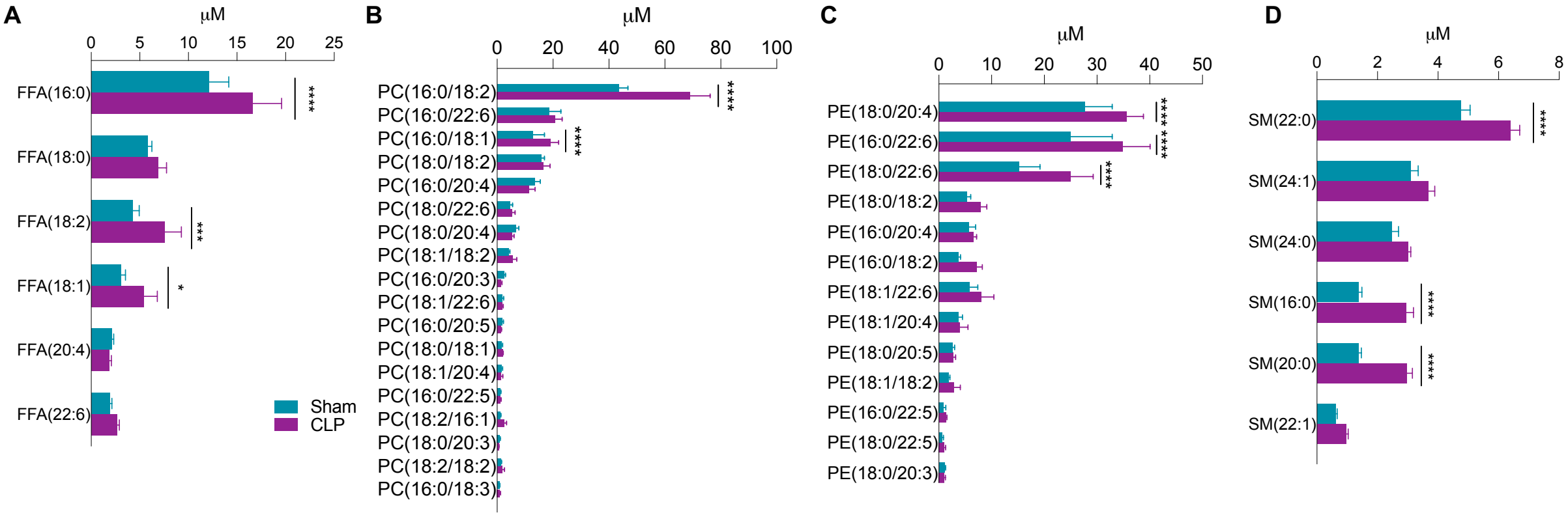

Supplemental figure 4: Phosphatidylcholine, phosphatidylethanolamine, and sphingomyelin quantifications. Ultrahigh Performance Liquid Chromatography-Tandem Mass Spectroscopy measurement of **(A)** free fatty acid species, **(B)** phosphatidylcholine species, **(C)** phosphatidylethanolamine species and **(D)** sphingomyelin species from isolated hepatocytes 30 hours post-surgery. n=5 sham, n=8 CLP. **** denotes $p<0.0001$ determined by two-way ANOVA followed by multiple comparisons test.

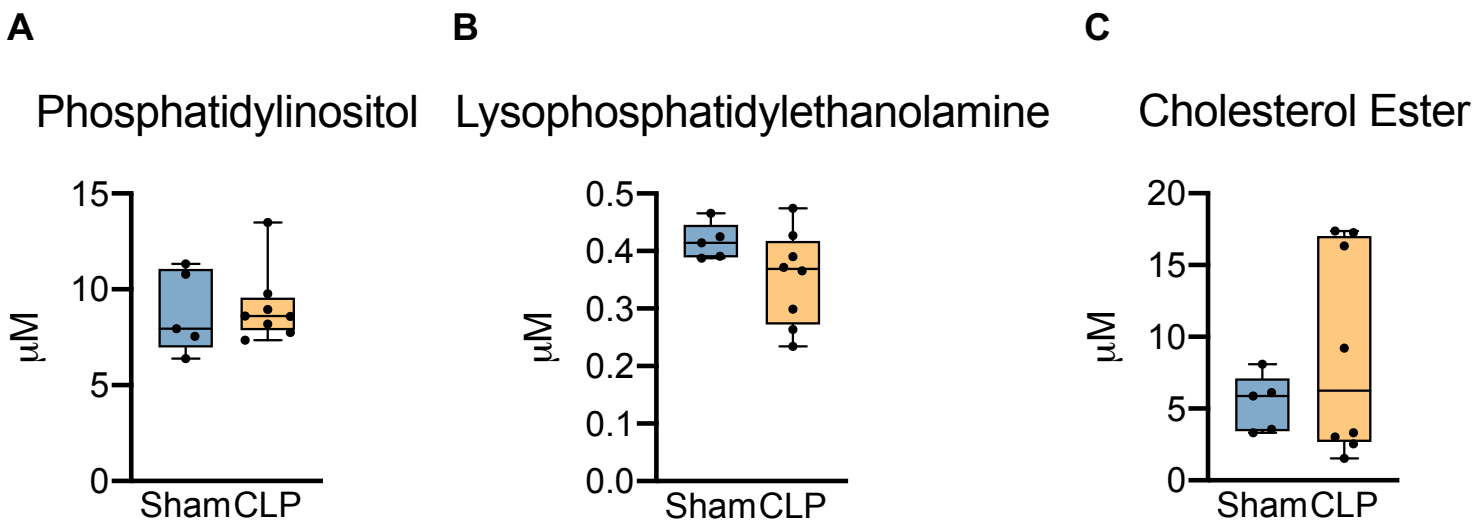

Supplemental figure 5: PI, LPE and CE levels in septic livers. Ultrahigh Performance Liquid Chromatography-Tandem Mass Spectroscopy measurement of **(A)** phosphatidylinositol, **(B)** lysophosphatidylethanolamine species and **(C)** cholesterol ester from isolated hepatocytes 30 hours post-surgery. n=5 sham, n=8 CLP. **** denotes $p<0.0001$ determined by two-way ANOVA followed by multiple comparisons test.